Novel infrared spectroscopic method for the determination of crystallinity of hydroxyapatite minerals

Nancy Pleshko, Adele Boskey* and Richard Mendelsohn
Department of Chemistry, Rutgers University, Newark College of Arts and Science, Newark, New Jersey, 07102; and
*Department of Ultrastructural Biochemistry, Cornell University Medical College and the Hospital for Special Surgery, New York, New York, 10021 USA

ABSTRACT Biologically important apatite analogues have been examined by Fourier Transform Infrared Spectroscopy (FT-IR), and a method developed to quantitatively assess their crystallinity. Changes in the phosphate ν_1 and ν_3 regions, 900–1,200 cm^{-1}, for a series of synthetic (containing hydroxide, fluoride, or carbonate ion) and biological apatites with crystal sizes of 100–200 Å were analyzed with curve-fitting and second derivative spectroscopy. The ν_1,ν_3 contour was composed of three main subbands. Correlations were noted between two spectral parameters and crystal size as determined by x-ray diffraction. The percentage area of a component near 1,060 cm^{-1} decreased as the length of the c-axis of the hydroxyapatite (HA) compounds increased, while the frequency of a band near 1,020 cm^{-1} increased with increasing length of the apatite c-axis. These parameters are thus proposed as indices of crystallinity for biological (poorly crystalline) HA. The FT-IR spectra of highly crystalline apatitic compounds were also analyzed. For crystal sizes of 200–450 Å, the percentage area of the phosphate ν_1 band (near 960 cm^{-1}) decreased with increasing HA crystal size. IR indices of crystallinity have thus been developed for both well crystallized and poorly crystallized HA derivatives. The molecular origins of the various contributions to the ν_1,ν_3 contour are discussed, and a preliminary application of the method to a microscopic biological sample (rat epiphyseal growth plate) is illustrated.

INTRODUCTION

Poorly crystalline hydroxyapatite (HA) is the major mineral component of bone and other physiologically calcified tissues. Studies of HA in synthetic analogues as well as tissues have revealed many structural details (for reviews, see, for example, Bailey and Holt, 1989; Berry, 1967; Fowler, 1974*a*; LeGeros, 1981; Posner et al., 1979). Stoichiometric HA, $Ca_{10}(PO_4)_6(OH)_2$ in its most common form, occurs as a hexagonally packed crystal. Apatite from biological tissues is carbonate substituted, ~5–6% by weight (LeGeros, 1981). The $CO_3^=$ ion can substitute for either the phosphate or the hydroxyl groups of HA, leading to a nonstoichiometric apatite mineral (Bonel, 1972*a*, *b*; Elliot, 1961; Emerson and Fischer, 1962). Other possible substitutions include replacement of the hydroxyl group by fluoride ion. This may be an important event during the treatment of the bone disease osteoporosis with NaF (Gron et al., 1966).

The structure of HA analogues have been extensively studied by various chemical and physical methods (Blumenthal et al., 1975; Eanes et al., 1973; Fowler et al., 1966; Posner et al., 1979; Termine and Lundy, 1973). In particular, the crystallinity, i.e., crystal size and perfection, of apatites are of great biomedical interest, because smaller, more imperfect crystals, being subject to dissolution, may effect the extent of bone loss in osteoporosis and other metabolic bone diseases (Thompson et al., 1983). Traditionally, x-ray diffraction is the technique of choice for determination of apatite crystal size. The method, while direct, cannot be applied to microscopic samples with rapid spatial variation in mineral structure such as biological tissue specimens.

In contrast, structural information relating to the apatite mineral in macroscopic, as well as microscopic samples, can be readily obtained from IR spectroscopy. Termine and Posner (1966) developed an IR method to determine the percentage of crystallinity in apatite minerals, based on changes in the phosphate ν_4 mode. Others have carried out analyses of calcium phosphates to determine the molecular species contributing to the characteristic phosphate bands (Baddiel and Berry, 1966; Bhatnagar, 1988; Cant et al., 1971; Fowler et al., 1966; Fowler, 1974*a*, *b*; Stutman et al., 1965). Fourier deconvolution techniques have recently been used to analyze spectra of both synthetic and biological calcium phosphates (Rey et al., 1991; Rey et al., 1990).

This study describes a novel IR method to assess the crystallinity of HA minerals, based on changes in the phosphate ν_1 and ν_3 absorbances in the 900–1,200-cm^{-1} spectral region. The technique is suited to both macro- and microscopic samples, and serves to complement x-ray diffraction analysis of crystal size and perfection. The method, developed from spectra of biologically-relevant hydroxyl, carbonate, and fluoride-substituted apatites of known crystal sizes, was then employed to determine the crystal size of apatite in rat femur epiphyseal growth plates, a problem not readily addressed by x-ray diffraction techniques.

0006-3495/91/10/786/08 $2.00

EXPERIMENTAL

Materials

Poorly crystalline HA was prepared from amorphous calcium phosphate (ACP) in 0.15 M Tris buffer at room temperature, pH 8.5 (Boskey and Posner, 1973). Carbonate-substituted HA was prepared from ACP in a solution containing 0.15 M Tris and 0.026 M Ca_2CO_3 at pH 8.5 or 7.4, (Blumenthal et al., 1975). Fluoride-substituted HA was prepared by the addition of NaF to ACP in solution, pH 8.5 (Hasvold and Dahm, 1977). Ca/F mole ratios of 10 to 1, and 5 to 1, respectively, were used. For each reaction mixture, aliquots of the slurry were removed at sequential time points (ranging from time "0", start of the reaction, to 3 wk), filtered, washed with pH 10 water, and dried with acetone. The precipitate was dried under vacuum overnight, and stored desiccated until use. KBr pellets of the precipitates were prepared using 0.5 mg sample/100 mg KBr, and their FT-IR spectra recorded. The carbonate content of the compounds was determined by the Conway microdiffusion method (Conway, 1957), and the fluoride content determined by measurement with a fluoride specific ion electrode.

Well crystallized apatites examined included geological fluorapatite and chlorapatite, hydroxyapatite prepared by refluxing, and carbonate substituted apatite prepared at 37°C (kindly supplied by Dr. R. LeGeros, New York University School of Dental Medicine, New York).

Bone samples were ground in a liquid nitrogen cooled colloid mill (Spex Industries, Metuchen, NJ), and sieved through a metal 325 μ mesh. KBr pellets for IR examination of ground bone were prepared using 0.5 mg sample/100 mg KBr.

Thin (5 μ) rat femur sections were cut on a Tissue-Tek No. 2 Cryostat (Electrobiology, Inc., Fairfield, NJ) equipped with an American Optical steel microtome knife.

Methods

FT-IR spectroscopy. FT-IR spectra were recorded with a SIRIUS 100 spectrophotometer (Mattson Instruments, Inc., Madison, WI), equipped with a Bach-Shearer FT-IR microscope and a Mercury-Cadmium-Telluride detector. Routinely, 400 interferograms were collected, coadded, apodized with a triangular function, and fast Fourier transformed to yield spectra with 4 cm^{-1} resolution with data encoded every 2 cm^{-1}.

X-ray diffraction. The structure of the apatites were confirmed by wide angle x-ray diffraction, using Cu K-α radiation on a Siemens automated powder diffractometer (Siemens-Allis Inc., Cherry Hill, NJ). Crystallinity was assessed from the line broadening of the 002 (*c*-axis) reflection.

Data analysis

Crystal sizes of the apatites were calculated from x-ray diffraction line width data. The width at half height of the 002 reflection, β_{002}, is inversely proportional to the crystallite length along the c unit cell direction (Cullity, 1956), which is termed the "*c*-axis length" in this study, as follows.

$$D = \frac{0.9\lambda}{\beta_{002}\cos\theta},$$

where D is the crystal size (Å); λ is the wavelength of the incident x-rays, 1.54 Å; β_{002} is the width at half height of the 002 reflection; and cosθ is the cosine of the x-ray incident angle (25.85°).

The 900–1200-cm^{-1} IR spectral region contains the phosphate symmetric and antisymmetric stretching vibration, ν_1 and ν_3, respectively. Analysis of the contour was carried out with software developed at the National Research Council of Canada, Ottawa, and generously supplied by D. Moffatt. The curve-fitting algorithm creates Lorentzian-Gaussian bands that are added to produce a computed spectrum, which is compared with the experimental spectrum. The process is iterated until a satisfactory fit between the computed and experimental band is obtained by a least squares regression analysis. The calculated area of each subband is reported as a percentage of the computed contour. Initial peak positions were obtained from second-derivative spectra of the raw data (Fig. 1 *A*). The relative proportions of Lorentzian-Gaussian bandshapes are varied for the set of subbands during the iteration.

Because the analysis depends on the positions and intensities of the components of the contour, substantial attention was paid to obtaining the best possible fit with the minimum number of component bands. It was evident from the second derivative spectra (see Fig. 1 *A* for an example) that at least four bands were required. Initial iterations produced obvious difference patterns which guided the selection of the remaining two features. The effect of the number of bands on the

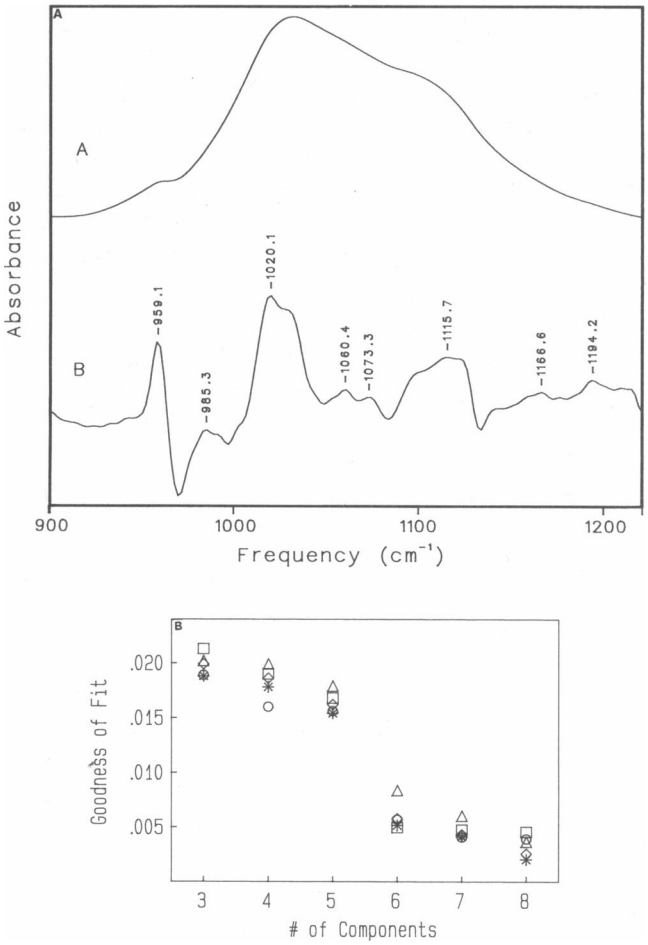

FIGURE 1 (*A*) Typical FT-IR spectrum of poorly crystalline hydroxyapatite, phosphate ν_1,ν_3 region. Second derivative spectrum (*B*) shows at least four underlying components. (*B*) Goodness of fit versus number of components used in the curve fit analysis of poorly crystalline carbonate-substituted apatites. Circle, 90 min in solution; square, 3 h; asterisk, 24 h; diamond, 72 h; triangle, 3 wk.

quality of the fit for five separate samples is shown in Fig. 1 *B*. In each case, the goodness-of-fit (GOF) parameter from the least squares algorithm (the normalized root mean square deviation), was determined as a function of the number of bands used for the fit. In all cases, the improvement in GOF diminishes drastically with addition of a seventh component (Fig. 1 *B*); it was thus evident (and consistent results for more than 100 data sets were obtained using this criterion) that six bands were both necessary and sufficient to accurately represent the contour of poorly crystalline apatites.

RESULTS

Spectral changes accompanying HA crystal growth were evaluated during the solution-mediated transformation of amorphous calcium phosphate (ACP), $Ca_3(PO_4)_2 \cdot XH_2O$, to HA, $Ca_{10}(PO_4)_6(OH)_2$. ACP undergoes an autocatalytic reaction in aqueous solution to form a poorly crystalline HA (Boskey and Posner, 1973), resulting in crystals ranging in size from 100 to 200 Å. As the HA crystals mature, the IR spectra of the calcium phosphate precipitates taken at sequential time points are substantially altered (Fig. 2). Qualitatively, the shape of the ν_1,ν_3 absorbance progressively changes from the broad, generally featureless (except for the shoulder at 960 cm^{-1}) contour seen in ACP, to a composite of overlapping narrower bands from which a high frequency shoulder eventually emerges. The broad ν_4 absorbance band in the 500–700-cm^{-1} region also becomes resolved into two distinct peaks, characteristic of

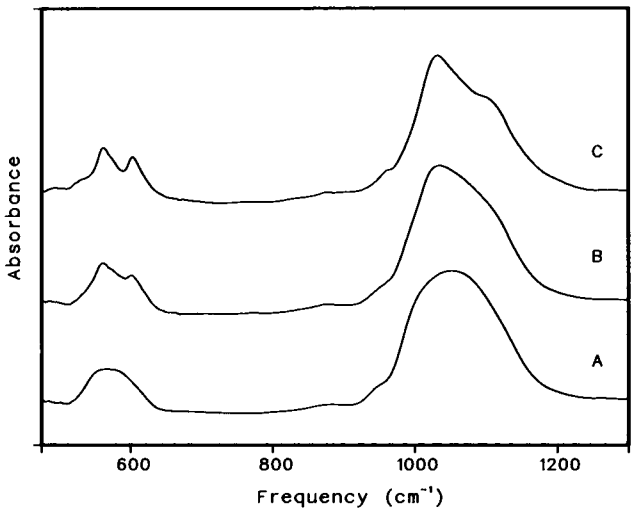

FIGURE 2 FT-IR spectra showing the solution-mediated, autocatalytic conversion of amorphous calcium phosphate (ACP) to poorly crystalline HA. *A*: ACP; *B*: HA, in solution 90 min; *C*: HA, 24 h in solution. With time, the phosphate ν_1,ν_3 region (900–1,200 cm^{-1}) changes from a broad band, as in ACP, to a narrower band with a high frequency shoulder. The ν_4 region (500–700 cm^{-1}) becomes resolved into two distinct peaks.

hydroxyapatite. As noted above, we have correlated changes in the 900–1,200-cm^{-1} region with the size (c unit cell dimension) of the HA crystals.

Because biological apatites contain ~5–6% carbonate by weight, it was deemed useful to include carbonate-substituted apatites in this study. In addition, the widespread use of fluoride as a therapeutic agent in the treatment of osteoporosis (Baud et al., 1988; Gron et al., 1966; Kragstrup et al., 1989), led us to examine fluoride-substituted materials.

The spectral features between 900 and 1,200 cm^{-1} arise primarily from the symmetric (ν_1) and antisymmetric (ν_3) P-O stretching modes of the ACP and HA phosphate groups. Under strict tetrahedral symmetry for orthophosphate, ν_1 is IR inactive. However, when the symmetry in the crystal is lowered from that of the free ion (e.g., in HA), the symmetric stretch appears as a weak feature in the IR spectra between 950–970 cm^{-1}. The ν_3 mode is triply degenerate in the free ion, and may resolve into three separate modes when the degeneracy is lifted. We therefore expect that analysis of the 900–1,200-cm^{-1} region would lead to multiple bands arising from both the phosphate ν_1 and ν_3 modes.

Bands in the 500–700-cm^{-1} region arise primarily from the antisymmetric P-O bending modes of the phosphate groups. This triply degenerate mode (F_2 in T_d symmetry), is resolved into at least two well defined peaks in HA (Baddiel and Berry, 1966). Analysis of this spectral region produced no conclusive spectra-structure correlations.

The weak absorbance band at ~870 cm^{-1} arises primarily from ν_2 (A_2'') of carbonate (Termine and Lundy, 1973), which may be incorporated into the apatites from atmospheric CO_2. Without addition of $CaCO_3$ to the ACP reaction mixture, the carbonate content of the HA was ~2% by weight after 3 wk in solution.

Fig. 3 displays spectra representative of poorly crystalline HA, with the experimental and calculated contours overlaid along with the individual subbands. Six components were necessary and sufficient for a suitable fit in the 900–1,200-cm^{-1} spectral region, with the three main features near 1,020, 1,050, and 1,110 cm^{-1} being termed the A, B, and C marker bands, respectively. Similar results were obtained for carbonate and fluoride substituted apatites, respectively (Fig. 4). The position, intensity, and linewidth of each component were examined. Correlations were noted between two of the parameters (the fractional intensity of the B band, and the position of the A band) with crystal size of the apatites.

The principal relationship was a decrease in the percentage area of component B, from ~45 to 5%, as the crystal size of the apatites increased from ~135 to 190 Å (Fig. 5 *A*). From these data it is clear that a

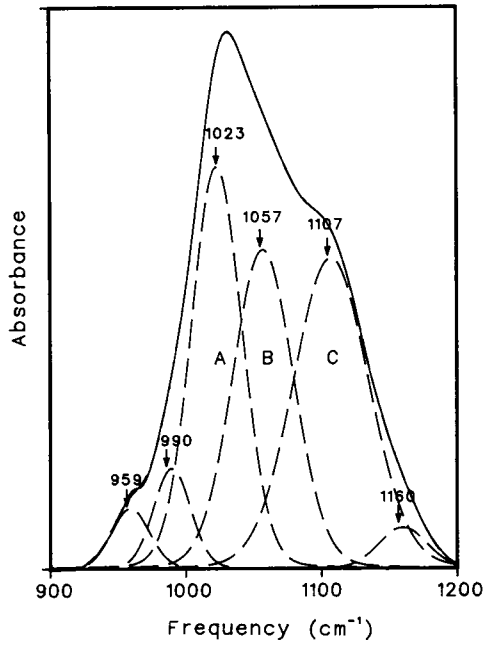

FIGURE 3 Typical FT-IR spectrum of poorly crystalline HA, phosphate ν_1,ν_3 region (—), with an overlay of the calculated contour, and the individual components (- - - - -) as determined by a curve fitting analysis. Six components were needed for a satisfactory fit, of which components *A*, *B*, and *C* were the main features of the contour.

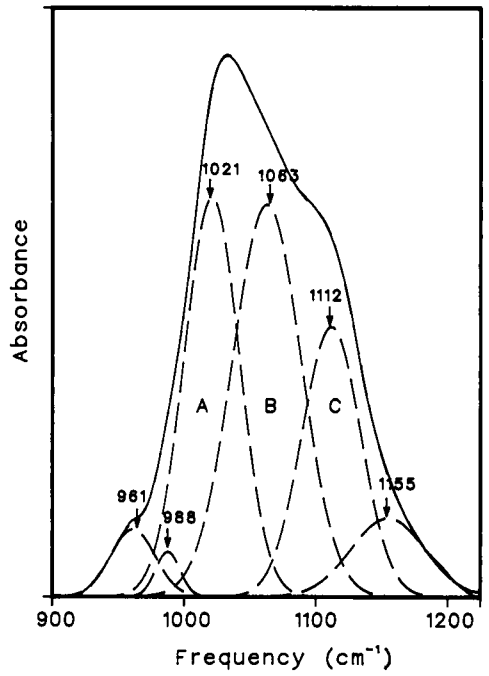

FIGURE 4 Typical FT-IR spectrum of a carbonate-substituted HA (4.5% carbonate by weight), phosphate ν_1,ν_3 region (—), with an overlay of the calculated contour, and the individual components (- - - - -) as determined by a curve fitting analysis.

different spectral parameter is required for crystal sizes > 200 Å, because as the area of the B band is diminished in intensity, it becomes too difficult to measure accurately. However, for apatites with sizes in this range, knowledge of the percentage area of component B gives a useful indication of crystal size. Thus, an index of crystallinity of poorly crystalline HA compounds, regardless of atomic (chemical) substitution, has been developed.

To verify that the index of crystallinity is applicable to biological materials, FT-IR spectra were collected from KBr pellets of four different ground bone samples, including rat, bovine, and rabbit bone (whose principal mineral component in each instance is a poorly crystalline HA [LeGeros, 1981]). The 900–1,200-cm^{-1} region for each spectrum was curve fit, and the percentage area component B versus the crystal size datum for each sample is included in Fig. 5 *A*. The data agree extremely well with those from the model compounds, demonstrating that the correlation extends to biological samples. Nonlinear regression analysis of the data in Fig. 5 *A* led to the following relationship between fractional area of the B band and *c*-axis crystal size:

$$Y = aX^b + c \qquad (r = 0.84)$$

Y = Crystal size (Å)

X = Percentage area component B

$a = -30.70$

$b = 0.2840$

$c = 227.8.$ (1)

The quantitative correlation proposed above is valid for interpolation purposes for c unit cell lengths between 195 and 135 Å. A second semiquantitative relationship is apparent between the frequency of the A component and the crystal size of the apatites. The frequency is not greater than 1,027-cm^{-1} for apatite crystal sizes less than ~160 Å, and increases to 1,028–1,032-cm^{-1} for crystal sizes between ~160–190 Å. This parameter is thus appropriate as a secondary indicator of crystal size for poorly crystalline specimens. The remaining four components of the contour could not be related to HA crystal size.

Well crystallized apatites (200–450 Å in size) revealed additional spectral features compared with the more poorly crystalline materials. Fig. 6 shows a spectrum typical of a well crystallized apatite in the 900–1,200-cm^{-1} region. Qualitatively, the central contour is considerably narrower than that of the poorly crystalline HA, with the high frequency shoulder more clearly defined. The band requires at least eight components for an

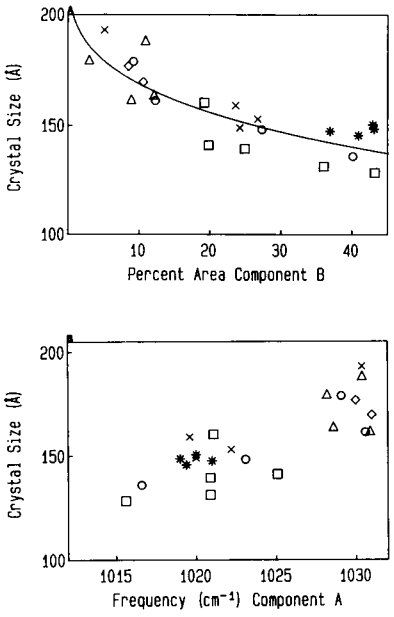

FIGURE 5 (*A*) Relationship of crystal size (Å) (*c*-axis dimension) to percentage area component B, and (*B*) to the position of component A (see Fig. 3) as determined by curve fitting analysis, for a series of poorly crystalline apatite analogues in the 100–200 Å range. HA, prepared at pH 8.5 (○); carbonate-substituted HA, prepared at pH 8.5 (□); carbonate-substituted HA, prepared at pH 7.4 (*); fluoride-substituted HA, prepared at pH 8.5 (◇); fluoride-substituted HA, prepared at pH 7.4 (△); biological samples, as discussed in the Experimental section (x).

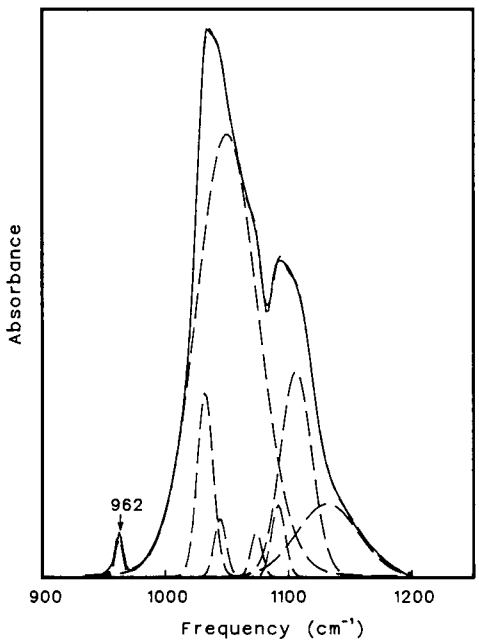

FIGURE 6 Typical FT-IR spectrum of a well crystallized apatite, HA prepared by refluxing for 24 h (—), with an overlay of the calculated contour, and the individual components (- - - - -), as determined by a curve-fitting analysis. Eight components were needed for a satisfactory fit.

adequate fit to the spectrum, compared with only six in the less crystalline preparations. Due to the additional features, it was not realistic to attempt to identify particular components characteristic of mineral size in this series of materials. However, a correlation (Fig. 7) was found between the percentage area of the ν_1 band (near 960 cm^{-1}) and crystal size. The ν_1 component decreases from ~1.9 to 0.5% as crystal size increases from ~200 to 450 Å. This constitutes a useful index of crystallinity for well crystallized apatites.

We note that it is easy to determine which type of apatite, poorly or well crystallized, one is analyzing, and therefore which of the available spectral indices are appropriate for crystal size determination. The contour in the 900–1,200-cm^{-1} spectral region is much narrower for the well crystallized apatites (crystal size >200 Å), and the ν_1 component is clearly resolved. Biological apatites generally have crystal sizes comparable to the poorly crystalline preparations examined in this study, and therefore the "A" and "B" components derived from the data analysis yield the appropriate indices of crystallinity.

The utility of this method for HA crystal size determination is demonstrated through FT-IR microscopy studies of thin (5 μ), sagittal rat femur sections. FT-IR spectra were collected from discrete areas, 30 μ in diameter, of the femur epiphyseal growth plate, where the newest mineral is formed (Warshawsky, 1982). Examination of the 900–1,200-cm^{-1} spectral regions reveal obvious qualitative differences in the contour of this band, corresponding to distinct regions of the growth plate. Application of the method described above for crystal size determination led to quantitation of the apatite mineral dimension at various regions of

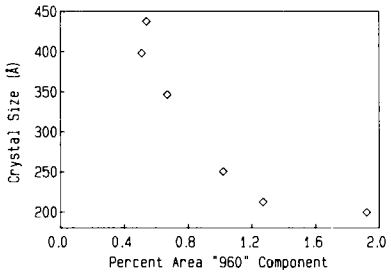

FIGURE 7 Relationship of crystal size (Å) (*c*-axis dimension) to percentage area ν_1 component as determined by curve-fitting analysis, for a series of well crystallized apatite analogues, including fluorapatite, chlorapatite, apatite prepared by refluxing, and carbonate-substituted apatites prepared at 37°C.

growth plate (Fig. 8 *A*, *B*). Although detailed interpretation of the biomedical and developmental significance of these results will be deferred for a more appropriate forum, it is clear that we have obtained information about the crystallinity of the mineral at 30 μ spatial resolution, an experiment not feasible for conventional x-ray diffraction techniques.

DISCUSSION

A spectroscopic method has been developed to assess the crystallinity of hydroxyapatite minerals. The observed changes in the 900–1,200-cm^{-1} spectral region, which reflect the maturation of HA crystals, have been quantitated by a least squares curve fitting analysis. Six components were needed to obtain a satisfactory fit for the poorly crystalline apatites studied (125–190 Å), whereas seven or eight components were needed to fit the well crystallized apatite (200–450 Å in size) spectra. A discussion of the possible molecular origin of the components follows.

The phosphate ion, PO_4^{3-}, is the principal molecular species giving rise to the HA absorbance in the 900–1,200-cm^{-1} region. Fowler et al. (1966) have characterized the infrared frequencies of HA. The ν_1 absorbance occurs at 962 cm^{-1}, while two components of ν_3, at 1,040 and 1,092 cm^{-1}, were identified.

The relationship demonstrated here between two components of the ν_1,ν_3 contour, and the crystal size of the poorly crystalline apatite minerals may be used to aid in the assignment of the phosphate ion bands. The percentage area of component B, centered near 1,060 cm^{-1}, was shown to decrease as the apatite *c*-axis length increased from ~135 to 195 Å. Because component B is largest for the apatite mineral of smallest crystal size, this element of the contour presumably arises from a disordered phosphate phase not located in the crystalline environment.

The frequency of component A of the 900–1,200-cm^{-1} contour increases from ~1,015 to 1,030 cm^{-1}, as crystal size of the poorly crystalline HA increases from ~125 to 190 Å. It is probable that this component, together with component C centered near 1,105 cm^{-1}, represent two elements of the ν_3 mode, whose degeneracy is lifted by the local symmetry of the HA crystal lattice. A previous study of apatite minerals, using Fourier self-deconvolution techniques, has attributed a 1,020-cm^{-1} band to nonstoichiometric apatite containing HPO_4^{2-} and CO_3^{2-}, and an 1,125-cm^{-1} band to stoichiometric apatite (Rey et al., 1991). These results are in agreement with the present study which indicates that the frequency of component A is reduced for less crystalline apatite minerals.

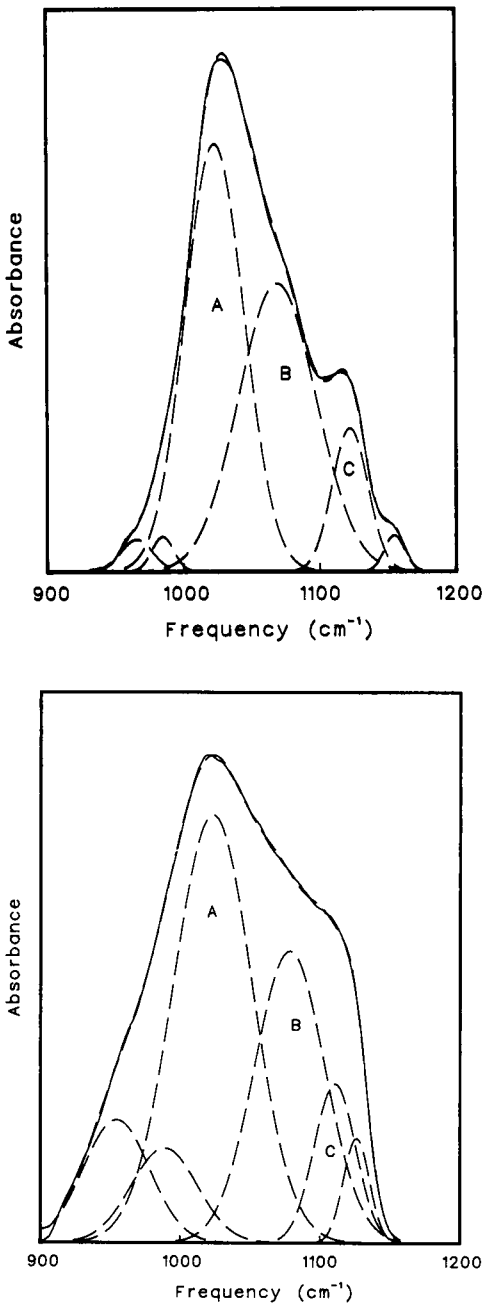

FIGURE 8 (*A*) FT-IR microscopy spectrum, 30 μ diameter region, taken from a region of calcified cartilage in the rat femur epiphyseal growth plate (—), with an overlay of the calculated contour and the individual components (- - - -), as determined by a curve-fitting analysis. Using the percentage area component B, 38.6%, and Eq. 1, the crystal size of the apatite mineral was estimated to be 141 Å. (*B*) FT-IR microscopy spectrum, 30 μ diameter region, taken from a region ~40 μ below that of part A (—), with an overlay of the calculated contour and the individual components (- - - -), as determined by a curve-fitting analysis. Eq. 1 and percentage area component B, 26.3%, were used to estimate the crystal size of the mineral in this region (150 Å).

A contribution from the phosphate ion of HPO_4^{2-} in the 900–1,200-cm^{-1} absorbance of HA is also possible. Many studies have identified HPO_4^{2-} in biological and synthetic apatites, either incorporated into the crystal lattice, or on the surface of the HA (Arends and Davidson, 1975; Berry, 1967; Termine and Eanes, 1972). The free HPO_4^{2-} ion has C_{3v} symmetry, leading to eight normal modes of vibration (Table 1). The symmetric ν_2 A mode and the doubly degenerate ν_6 E P-O stretch appear in the 900–1,200-cm^{-1} region, at 988 and 1,076 cm^{-1}, respectively. When this ion is incorporated into a crystal lattice, as in brushite, $CaHPO_4 \cdot 2H_2O$, the ν_2 mode appears as a doublet, at 987 and 1,000 cm^{-1}, and the ν_6 mode appears between 1,058 and 1,137 cm^{-1} (Berry and Baddiel, 1967). Accordingly, it is possible that two of the components of the 900–1,200-cm^{-1} region obtained by the curve fit analysis arise from HPO_4^{2-} modes, indicating incorporation of the acid phosphate in the apatite lattice, or on its surface. The high frequency component near 1,140 cm^{-1}, and the component near 989 cm^{-1} may both arise from HPO_4^{2-}.

The carbonate ion may incorporate into the HA lattice at two different positions, known as the "A" (hydroxyl substitution) and "B" (phosphate substitution) sites (Bonel, 1972*a*, *b*; Elliot, 1961; Emerson and Fischer, 1962). Much work has been carried out to determine the effects of CO_3^{2-} substitution on the infrared spectra of apatites (Blumenthal et al., 1975; Elliot et al., 1985; LeGeros et al., 1968). It is known that the ν_3 absorbance band is broadened by incorporation of carbonate into the HA lattice. Additionally, the phosphate environment of type B carbonate-apatites is probably altered, leading to more than one type of phosphate absorbance from the apatite. However, it was not possible to correlate carbonate substitution with any of the components of the 900–1,200-cm^{-1} region.

Fluoride is incorporated into the apatite lattice by means of substitution for the hydroxyl ion, causing an increase in crystal size by virtue of better packing of the crystal lattice (Posner et al., 1963; Schraer et al., 1962; Zipkin et al., 1962). Comparison of the fluoride substituted apatites to the unsubstituted apatites at equivalent reaction time points shows the fluorapatites to have a slightly larger crystal size (Fig. 5 *A*).

TABLE 1 HPO_4^{2-} vibrational modes*

P-O stretch	ν_2A	988
O-P-O bend	ν_8E	394
P-O(H) stretch	ν_3A	862
P-O stretch	ν_6E	1076
O-P-O bend	ν_4A	586
O-P-O bend	ν_7E	537
(P−)O-H stretch	ν_1A	2900
P-O-H bend	ν_5E	1230

*Bailey and Holt, 1989.

A relationship was established between the percentage area of the phosphate ν_1 mode, and the crystal size of the well crystallized apatite analogues (Fig. 7). The origin of the additional components needed to adequately fit for this series of compounds is unknown, but it is reasonable to assume that coupled corresponding motions of phosphate ions in the apatite lattice contribute to the absorbances in the 900–1,200-cm^{-1} region. Although it is unclear why the ν_1 absorbance decreases with increasing crystallinity of the well crystallized apatites, the relationship is empirically useful for determining the crystal size of compounds in the 200–450-Å region.

This spectroscopic method for determining the crystal size of HA analogues is valuable for experimental conditions where x-ray diffraction experiments cannot be performed. It is noted that the two methods do not provide exactly the same type of molecular information. However, the FT-IR data from the biological specimens agrees with previously reported crystallite size determination for comparable samples (Boskey and Marks, 1985).

IR spectroscopy and x-ray diffraction are thus both suited to determine crystal sizes greater than 100 Å, and should be used in conjunction when possible to obtain the maximum amount of structural information. When x-ray diffraction of apatites cannot be performed, as is the case with thin, calcified, spatially inhomogeneous tissue sections, or in the case of poorly crystalline substances, the method developed here is valuable for assessing the crystallinity of HA phases.

CONCLUSIONS

A novel infrared spectroscopic method has been developed to assess the crystallinity of poorly crystalline (crystal sizes of 100–190 Å) and well crystallized (200–450 Å) HA analogues, based on changes in the phosphate ν_1 and ν_3 absorbance. The technique is appropriate for the analysis of apatite minerals in both macroscopic samples and in microtomed calcified tissue sections. A preliminary application to the determination of the crystal size of apatite in a thin rat femur has been demonstrated.

The authors thank Dr. Steven Doty and Mr. Michael Maresca for their technical assistance.

Supported by National Institutes of Health grant DE-04141 and the Busch Memorial Fund of Rutgers University.

Received for publication 20 March 1991 and in final form 21 June 1991.

REFERENCES

Arends, J., and C. L. Davidson. 1975. HPO_4^{2-} content in enamel and artificial carious lesions. *Calcif. Tiss. Res.* 18:65–79.

Baddiel, C. B., and E. E. Berry. 1966. Spectra-structure correlations in hydroxy and fluorapatite. *Spectrochim. Acta.* 22:1407–1416.

Bailey, R. T., and C. Holt. 1989. Fourier transform infrared spectroscopy and characterisation of biological calcium phosphates. *In* Calcified Tissues. D. W. L. Hukins, editor. MacMillan Press, Houndmills, Basingstoke, Great Britain. 93–120.

Baud, C. A., J. M. Very, and B. Courvoisier. 1988. Biophysical study of bone mineral in biopsies of osteoporotic patients before and after long-term treatment with fluoride. *Bone.* 9:361–365.

Berry, E. E. 1967. The structure and composition of some calcium-deficient apatites. *J. Inorg. Nucl. Chem.* 29:317–327.

Berry, E. E., and C. B. Baddiel. 1967. The infra-red spectrum of dicalcium phosphate dihydrate (brushite). *Spectrochim. Acta.* 23*a*: 2089–2097.

Bhatnagar, V. M. 1968. Infrared spectra of hydroxyapatite and fluorapatite. *Bull. Soc. Chim. France.* 1771–1773.

Blumenthal, N. C., F. Betts, and A. S. Posner. 1975. Effect of carbonate and biological macromolecules on formation and properties of hydroxyapatite. *Calcif. Tiss. Res.* 18:81–90.

Bonel, G. 1972*a*. Contribution a l'etude de la carbonation des apatites. Part I. *Ann. Chim.* 7:65–87.

Bonel, G. 1972*b*. Contribution a l'etude de la carbonation des apatites. Parts II and III. *Ann. Chim.* 7:127–144.

Boskey, A. L., and S. C. Marks, Jr. 1985. Mineral and matrix alterations in the bones of incisors-absent (*ia/ia*) osteopetrotic rats. *Calcif. Tissue Int.* 37:287–292.

Boskey, A. L., and A. S. Posner. 1973. Conversion of amorphous calcium phosphate to microcrystalline hydroxyapatite. A pH-dependent, solution-mediated, solid-solid conversion. *J. Phys. Chem.* 77:2313–2317.

Cant, N. W., J. A. S. Bett, G. R. Wilson, and W. K. Hall. 1971. The vibrational spectrum of hydroxyl groups in hydroxyapatites. *Spectrochim. Acta.* 27*A*:425–439.

Conway, E. J. 1957. Microdiffusion Analysis and Volumetric Error. Lockwood & Son Ltd., London.

Cullity, B. D. 1956. Elements of X-Ray Diffraction. Addison-Wesley Publishing Company, Inc., Reading, MA. 97–99.

Eanes, E. D., J. D. Termine, and M. U. Nylen. 1973. An electron microscopic study of the formation of amorphous calcium phosphate and its transformation to crystalline apatite. *Calcif. Tiss. Res.* 12:143–158.

Elliot, J. C., D. W. Holcomb, and R. A. Young. 1985. Infrared determination of the degree of substitution of hydroxyl by carbonate ions in human dental enamel. *Calcif. Tissue Int.* 37:372–275.

Elliott, J. C. 1961. The infrared spectrum of the carbonate ion in carbonate-containing apatites. (Abstr.) *J. Dent. Res.* 30:1284.

Emerson, W. H., and E. E. Fischer. 1962. The infra-red absorption spectra of carbonate in calcified tissues. *Arch. Oral Biol.* 7:671–683.

Fowler, B. O. 1974*a*. Infrared studies of apatites. I. Vibrational assignments for calcium, strontium, and barium hydroxyapatites utilizing isotopic substitution. *Inorg. Chem.* 13:194–207.

Fowler, B. O. 1974*b*. Infrared studies of apatites. II. Preparation of normal and isotopically substituted calcium, strontium, and barium hydroxyapatites and spectra-structure-composition correlations. *Inorg. Chem.* 13:207–214.

Fowler, B. O., E. C. Moreno, and W. E. Brown. 1966. Infra-red spectra of hydroxyapatite, octacalcium phosphate and pyrolysed octacalcium phosphate. *Arch. Oral Biol.* 11:477–492.

Gron, P., H. G. McCann, and D. Bernstein. 1966. Effect of fluoride on human osteoporotic bone mineral. *J. Bone and Joint Surg.* 48*A*:892–897.

Hasvold, Ö., and S. Dahm. 1977. The effect of fluoride on the transformation of amorphous calcium phosphate into crystalline apatite. *Calcif. Tiss. Res.* 22 (Suppl):425–427.

Kragstrup, J., Z. Shijie, L. Mosekilde, and F. Melsen. 1989. Effects of sodium fluoride, vitamin D, and calcium on cortical bone remodeling in osteoporotic patients. *Calcif. Tissue Int.* 45:337–341.

LeGeros, R. Z., O. R. Trautz, J. P. LeGeros, and E. Klein. 1968. Carbonate substitution in the apatite structure (1). *Bull. Soc. Chim. France.* 1712–1717.

LeGeros, R. Z. 1981. Apatites in Biological Systems. *Prog. Crystal Growth Charact.* 4:1–45.

Posner, A. S., F. Betts, and N. C. Blumenthal. 1979. Bone mineral composition and structure. *In* Skeletal Research. D. J. Simmons and A. S. Kunin, editors. Academic Press, New York. 167–192.

Posner, A. S., E. D. Eanes, R. A. Harper, and I. Ziplin. 1963. X-ray diffraction analysis of the effect of fluoride on human bone apatite. *Arch. Oral Biol.* 8:549–570.

Rey, C., M. Shimuzu, B. Collins, and M. J. Glimcher. 1991. Resolution enhanced fourier transform infrared spectroscopy study of the environment of phosphate ion in the early deposits of a solid phase of calcium phosphate in bone and enamel and their evolution with age. 2. Investigations in the ν_3 PO_4 domain. *Calcif. Tissue Int.* In press.

Rey, C., M. Shimuzu, B. Collins, and M. J. Glimcher. 1990. Resolution-enhanced fourier transform infrared spectroscopy study of the environment of phosphate ions in the early deposits of a solid phase of calcium-phosphate in bone and enamel, and their evolution with age. I. Investigations in the ν_4 PO_4 domain. *Calcif. Tissue Int.* 46:384–394.

Schraer, H., A. S. Posner, R. Schraer, and I. Zipkin. 1962. The effect of fluoride one bone "crystallinity" in the growing rat. *Biochim. Biophys. Acta.* 64:565–567.

Stutman, J. M., J. D. Termine, and A. S. Posner. 1965. Vibrational spectra and structure of the phosphate ion in some calcium phosphates. *Trans. NY Acad. Sci.* 27:669–675.

Termine, J. D., and E. D. Eanes. 1972. Comparative chemistry of amorphous and apatitic calcium phosphate preparations. *Calcif. Tiss. Res.* 10:171–197.

Termine, J. D., and D. R. Lundy. 1973. Hydroxide and carbonate in rat bone mineral and its synthetic analogues. *Calcif. Tiss. Res.* 13:73–82.

Termine, J. D., and A. S. Posner. 1966. Infra-red determination of the percentage of crystallinity in apatitic calcium phosphates. *Nature (Lond.)* 211:268–270.

Thompson, D. D., A. S. Posner, W. S. Laughlin, and N. C. Blumenthal. 1983. Comparison of bone apatite in osteoporotic and normal eskimos. *Calcif. Tissue Int.* 35:392–393.

Warshawsky, H. 1982. Embryology and development of the skeletal system. *In* The Musculoskeletal System Embryology, Biochemistry, and Physiology. R. L. Cruess, editor. Churchill Livingstone, New York. 33–56.

Ziplin, I., A. S. Posner, and E. D. Eanes. 1962. The effect of fluoride on the x-ray-diffraction pattern of the apatite of human bone. *Biochim. Biophys. Acta.* 59:255–258.